Marini, J. C., Levene, S. D., Crothers, D. M., & Englund, P. T. (1982) *Proc. Natl. Acad. Sci. U.S.A. 79*, 7664–7668.
Marini, J. C., Effron, P. N., Goodman, T. C., Singleton, C. A., Wells, R. D., Wartell, R. M., & Englund, P. T. (1984) *J. Biol. Chem. 254*, 5417–5422.
Marquardt, D. W. (1963) *J. Soc. Ind. Appl. Math. 11*, 431–441.
Peck, L. J., & Wang, J. C. (1981) *Nature (London) 292*, 375–378.
Prunell, A., Goulet, I., Jacob, Y., & Goutorbe, F. (1984) *Eur. J. Biochem. 138*, 253–257.
Selsing, E., Wells, R. D., Alden, C. J., & Arnott, S. (1979) *J. Biol. Chem. 254*, 5417–5422.
Simpson, R. T., & Kunzler, P. (1979) *Nucleic Acids Res. 6*, 1387–1415.
Sutcliffe, J. G. (1978) *Cold Spring Harbor Symp. Quant. Biol. 43*, 77–90.
Thomas, G. A., & Peticolas, W. L. (1983) *J. Am. Chem. Soc. 105*, 993–996.
Trifonov, E. N., & Sussman, J. L. (1980) *Proc. Natl. Acad. Sci. U.S.A. 77*, 3816–3820.
Wegener, W. A., Dowben, R. M., & Koester, V. J. (1979) *J. Chem. Phys. 70*, 622–632.
Wu, H.-M. (1982) Thesis, Yale University.
Wu, H.-M., & Crothers, D. M. (1984) *Nature (London) 308*, 509–513.
Yamakawa, H. (1970) *J. Chem. Phys. 53*, 436–443.
Zhurkin, V. B. (1985) *J. Biomol. Struct. Dyn. 2*, 785–804.
Zimm, B. H. (1980) *Macromolecules 13*, 592–602.

Proflavin Binding to Poly[d(A-T)] and Poly[d(A-br^{5}U)]: Triplet State and Temperature-Jump Kinetics†

Alan F. Corin‡ and Thomas M. Jovin*
Abteilung Molekulare Biologie, Max-Planck-Institut für Biophysikalische Chemie, D-3400 Göttingen, FRG
Received September 5, 1985; Revised Manuscript Received February 27, 1986

ABSTRACT: The delayed fluorescence properties of proflavin have been exploited in studies of the excited-state binding kinetics of the dye to poly[d(A-T)] and its brominated analogue poly[d(A-br^{5}U)] at room temperature and pH 7. The two analyzed luminescence decay times of the DNA–dye complex are dependent on the total nucleic acid concentration. This dependence is shown to reflect a temporal coupling of the intrinsic delayed emission decay rates with the dynamic chemical kinetic binding processes in the excited state. Temperature-jump kinetic studies conducted on the brominated polymer and corresponding information on poly[d(A-T)] from a previous study [Ramstein, J., Ehrenberg, M., & Rigler, R. (1980) *Biochemistry 19*, 3938–3948] provide complementary information about the ground state. In the ground state, the poly[d(A-T)]–proflavin complex has one chemical relaxation time, which reaches a plateau at high DNA concentrations. The brominated DNA–dye complex exhibits two relaxation times: a faster relaxation mode that behaves similarly to that for the unhalogenated DNA and a slower relaxation mode that is apparent at high DNA concentrations. The ground-state kinetic data are analyzed in terms of two alternative models incorporating series and parallel reaction schemes. The former consists of two sequential binding steps—a fast bimolecular process followed by a monomolecular step—while the latter consists of two coupled bimolecular steps. A similar analysis for the excited-state data yields reasonable kinetic constants only for the series model, which, in accordance with previous proposals for acridine intercalators, consists of a fast outside binding step followed by intercalation of the dye. A comparison of the ground- and excited-state kinetic parameters reveals that the external binding process is much stronger and the intercalation is much weaker in the excited state. That the excited-state data are only consistent with the series model suggests that delayed luminescence studies may provide a general tool for distinguishing between the two kinetic mechanisms. In particular, we demonstrate the use of delayed luminescence spectroscopy as a tool for probing dynamic DNA–ligand interactions in solution.

Acridine dyes exhibit a number of biologically interesting phenomena that have been the subject of extensive investigations. These planar heteronuclear chromophores demonstrate antibacterial (Albert, 1973) and mutagenic properties (Brenner et al., 1961; Streisinger et al., 1966) and are used as probes for visualizing chromosomes (Caspersson et al., 1969). Another useful feature of acridine–DNA interactions is the metachromasia exhibited by single- vs. double-stranded nucleic acids [Porumb, 1978; Peacocke (1973) and references cited therein].

Two modes of binding have been attributed to the acridine–DNA system at low dye concentrations (submicromolar) and DNA to dye (P/D)[1] ratios >10: (1) an external binding mode in which the electrostatic forces between the positively charged acridine (at neutral pH) and the polyanionic DNA polymer play a major role; (2) a stronger internal mode with

† A.F.C. was supported by a Max Planck Society fellowship.
‡ Present address: Life Sciences Division, Eastman Kodak Co., Rochester, NY 14650.

[1] Abbreviations: T jump, temperature jump; P/D, DNA (in nucleotide units) to dye ratio; Tris-HCl, tris(hydroxymethyl)aminomethane hydrochloride; EDTA, ethylenediaminetetraacetic acid.

0006-2960/86/0425-3995$01.50/0

the dye intercalated between the base pairs, as first proposed by Lerman (1961). At higher dye concentrations (>1 μM) and P/D ratios approaching 1, a model has been proposed whereby the nonintercalated dye is bound to single-stranded regions of the otherwise double-stranded helix such that the acridine molecules are sandwiched between consecutively unstacked bases (Kapuscinski & Daryznkiewicz, 1984; Kapuscinski et al., 1982).

A number of three-dimensional structures of acridines cocrystallized with self-complementary dinucleotides have been determined by X-ray crystallography [reviewed by Neidle & Berman (1983)] and provide information as to the spatial disposition of the intercalated species. Although no detailed geometric structural information exists to support intercalation in the case of binding of the drugs to longer DNA oligomers or polymers, its existence is inferred from a number of studies with double-stranded polynucleotides (Ramstein et al., 1972, 1973; Luzatti et al., 1961; Cairns, 1962; Mauss et al., 1967). A considerable degree of contour lengthening was shown to occur upon dye binding with the base pairs remaining roughly perpendicular to the helix axis (Lerman, 1963).

Studies of the binding kinetics of proflavin, a representative member of the acridine family, using the temperature-jump (T-jump) relaxation technique have revealed two binding steps with both (A-T)-rich naturally occurring DNA and synthetically prepared polymers (Li & Crothers, 1969; Ramstein & Leng, 1975; Ramstein et al., 1980). The same measurements on proflavin binding to (G-C)-rich polymers are consistent with a single-step binding mechanism. These studies utilized the fluorescence properties of the dye as a spectroscopic handle to monitor the ground-state binding kinetics. The short (nanosecond) lifetime of fluorescence from the singlet state ensures that the chemical relaxation kinetics, following a small temperature perturbation, is uncoupled to the decay of prompt fluorescence emission. Hence, the change in fluorescence quantum yield of proflavin as it binds provides a sensitive instantaneous indicator of the time-dependent reequilibration of the binding reactions in the ground state.

The small delayed luminescence from the triplet state of acridines at 25 °C in aqueous solution (with a quantum efficiency of phosphorescence $\Phi_p \sim 4 \times 10^{-6}$ and of delayed fluorescence $\Phi_{df} \sim 6 \times 10^{-5}$; Parker & Joyce, 1973) exhibits lifetimes in the microsecond to millisecond time range (Geacintov et al., 1981; Corin et al., 1985). Phosphorescence emission is the result of intersystem crossing from an excited singlet state to a lower energy excited triplet state followed by emission to the ground state. Delayed fluorescence involves thermal reactivation from the excited triplet state to the singlet state, which then emits. Thus, the delayed fluorescence displays the same emission spectrum characteristic of the prompt fluorescence while the phosphorescence spectrum is shifted to longer wavelengths. Following a pulse of excitation, both delayed emission processes decay with the relatively long lifetime corresponding to the triplet state. Ground-state proflavin intercalates into DNA with millisecond rates as determined from temperature-jump relaxation kinetic studies (Ramstein et al., 1980). We have performed a "light-jump" experiment on proflavin complexed to DNA analogous to the pulse and probe method of the T-jump technique. Previously, Geacintov et al. (1981) showed that the time course of the millisecond luminescence decay from the triplet state of proflavin bound to calf thymus DNA at room temperature is a function of the DNA concentration. The total delayed emission decay was analyzed in terms of one exponential, and the dependence of the lifetime upon the DNA concentration was attributed to the dynamic exchange between dye molecules free in solution and bound to the DNA. In a more recent study at lower P/D ratios (5–10), the luminescence decay was observed to contain up to three components (Corin et al., 1985).

In this work, the triplet decay of proflavin complexed to two synthetic polymers was measured. Observed decays were fit well by the sum of two exponentials and shown to be dependent on DNA concentration, implying a temporal coupling of the chemical, kinetic, and photophysical processes. Measurements on the ground-state binding dynamics of proflavin to poly[d(A-br^{5}U)] using the T-jump technique were performed. Excited- and ground-state data are compared and discussed in terms of kinetic models.

Experimental Procedures

Materials

Proflavin hemisulfate was purchased from Sigma Chemical Co. and used without further purification. Thin-layer chromatography in 5, 10, 20, and 40% methanol in chloroform showed no fluorescent-contaminating impurities. The concentrations of dye in stock solutions at pH 7.0 were determined spectrophotometrically with the extinction coefficient of 38 900 M^{-1} cm^{-1} at 444 nm (Albert, 1966).

DNAs. The synthetic polydeoxyribonucleotide poly[d(A-T)] was purchased from Boehringer Mannheim and P-L Biochemicals and dialyzed against a standard buffer composed of 10 mM Tris-HCl, 10 mM NaCl, and 0.1 mM EDTA, pH 7.0. Poly[d(A-br^{5}U)] was synthesized with *Micrococcal luteus* DNA polymerase I (P-L Biochemicals) by using a poly[d(A-T)] template and dATP and dbr^{5}UTP substrates as previously described by Gill et al. (1974) or purchased from P-L Biochemicals and subjected to dialysis before use. DNA concentrations (in nucleotide units) were measured spectrophotometrically with extinction coefficients of 6650 M^{-1} cm^{-1} at 260 nm and 5950 M^{-1} cm^{-1} at 266 nm for poly[d(A-T)] and poly[d(A-br^{5}U)], respectively (Inman et al., 1962).

All stock solutions were prepared in standard buffer. For each experiment on the luminescence spectrophotometer, fresh samples were prepared from concentrated stock solutions. For T-jump measurements of poly[d(A-br^{5}U)], the contents of the T-jump cell were diluted and reused when the DNA concentration exceeded 0.1 mM; otherwise, fresh solutions were prepared. The final NaCl concentration was 0.11 M for all measurements. Stock solutions were either kept at 4 °C for storage over several days or frozen at −20 °C for longer term storage. The DNA to dye ratio (P/D) was >50 for all T-jump and triplet-state measurements in order to avoid dye–dye interactions on the DNA helix.

Methods

Temperature-jump measurements were performed on the instrument of Drs. Ernst Grell and Horst Ruf in the Max Planck Institut für Biophysik (Frankfurt, FRG); it is similar to one previously described (Rigler et al., 1974). The main variation involved a prototype discharge circuit produced by Hilo-Test (Karlsruhe, FRG) which permits variable heating times by switching the discharge path of a 1.3-μF capacitor from the T-jump cell to ground after a predetermined time interval following the initiation of the discharge. In all experiments, a 25-kV discharge of 5-μs duration was selected, resulting in temperature jumps of 3.9 °C to a final temperature of 13.9 °C. Heating times of <10 μs were obtained in all cases. The fluorescence was excited at 436 nm with a 200-W Hg arc lamp and monitored through cutoff filters (KV550, G. Schott, Mainz) by two photomultiplier tubes at right angles to the excitation beam. After amplification, the signal was digitized

and stored in a 4K transient recorder memory (Nicolet Explorer-2090). The 1-mL T-jump cell had a 7-mm excitation path length. The data were transferred to a Hewlett-Packard computer and subsequently fit to mono-, bi-, and triexponential functions according to Provencher (1976a,b). Proflavin bleaches significantly on the second time scale. Therefore, an electronic light shutter placed in the excitation optical path was used to minimize exposure of the dye to unnecessary radiation.

Fluorescence titration of proflavin with poly[d(A-br^{5}U)] was conducted on an SLM Model 8000 spectrofluorometer (SLM Instruments Inc., Urbana, IL). To 600 μL of a 0.1 μM solution of proflavin were added successive aliquots of a 230 μM poly[d(A-br^{5}U)] stock solution; the fluorescence was excited at 450 nm and the spectrum scanned from 470 to 650 nm.

Triplet spectroscopic measurements were performed on an instrument that has been previously described (Austin et al., 1979; Jovin et al., 1981; Matayoshi et al., 1983; Corin et al., 1985). The excitation source was a Lambda Physik GmbH (Göttingen, FRG) excimer (XeCl, 307 nm) pumped dye laser, which delivers 10-ns tuneable pulses of light. For lifetime measurements, the laser dye Coumarin 307 (Lambda Physik) was used and the laser tuned to 493 nm with ~0.5 mJ/pulse. Emission was observed with an EMI 9817 QGB end-on photomultiplier tube through a combination of cutoff filters at 520 and 550 nm (KV520 and KV550, G. Schott, Mainz). Corion (Holliston, MA) narrow band-pass filters (10-nm bandwidth) were used to obtain spectrally resolved decay curves. After amplification, the luminescence signal was digitized by a Biomation Model 8100 transient recorder and subsequently stored and averaged in an Intel 8085 microprocessor system. Typically, 2048 channels of data were gathered for each of 2048 sweeps collected and averaged; the results were transferred to a PDP 11/23 minicomputer for analysis and display. Bleaching of the dye causes a loss of signal. Measures were taken in order to minimize this effect: (1) the laser beam was expanded 5-fold with a beam expander in order to reduce its energy density, and (2) the samples were constantly stirred by an overhead motor-driven propeller blade during data collection.

All solutions were purged of O_2, a paramagnetic triplet quencher, with a steady stream of argon, which flowed through a sintered glass frit submerged in water. The water-saturated gas was directed into the cuvette over the solution. The water saturation of argon reduces sample evaporation and, hence, changes in sample concentration. In order to determine the time required to obtain sufficient purging, decay measurements were made and analyzed until no further increase in the lifetime(s) could be observed.

Luminescence decay data were fit to a sum of exponentials utilizing two least-squares fitting programs, program 1 (Matayoshi et al., 1983) and program 2 (L. Avery, unpublished program), both of which employ the Marquardt fitting routine. The following strategy permitted weighting of the data according to a two-step procedure: the decay was first fit to two exponentials with no weighting (program 1); the reciprocal of this analysis curve served as the weighting function for a second fit (program 2). Using a fitted curve instead of the reciprocals of the experimental data points prevents the introduction of additional noise into the analysis. All curves were fit to the sum of one, two, and three exponential functions. In judging the adequacy of the analyses, the number of exponentials was increased until in the residuals plot there was neither a significant increase in the number of zero crossings nor a decrease in the sum of the squared residuals. By these criteria and by examination of an expanded overlay of the fitted and experimental curves, a biexponential function was deemed to be an adequate representation of the data. Furthermore, the third time derived from three-exponential fits did not show any systematic dependence upon DNA concentration. Despite electronic gating of the photomultiplier tube, the intense prompt fluorescence coincident with and immediately following the laser pulse induced a detector recovery time of ~100 μs. Consequently, all analyses were started 120 μs after the laser flash.

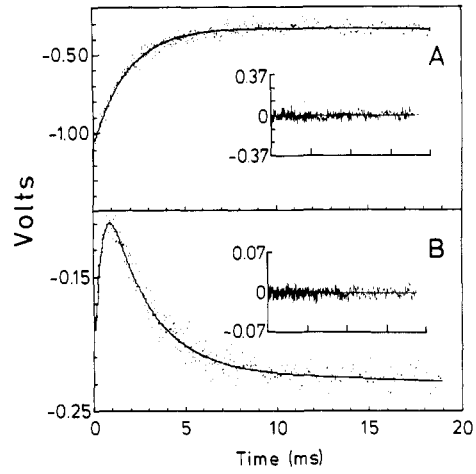

FIGURE 1: Representative T-jump relaxation curves of proflavin complexes with poly[d(A-br^{5}U)]: (A) 10 μM poly[d(A-br^{5}U)] and 0.1 μM proflavin (τ_{fast} = 1.86 ms); (B) 1.42 mM poly[d(A-br^{5}U)] and 1.0 μM proflavin (τ_{fast} = 0.24 ms, τ_{slow} = 1.71 ms). Buffer was 10 mM Tris-HCl, pH 7.0, 0.1 mM EDTA, and 0.11 M NaCl as in all subsequent figures. The ordinate is the fluorescence intensity in instrumental units (signal amplitude). The solid lines through the data are the fits, and the insets (ordinate axis in volts and abscissa divided into 5-ms divisions) are the corresponding residuals plots.

To collect time-resolved delayed luminescence spectra, the laser dye Stilbene 3 (Lambda Physik) was used and the laser tuned to 430 nm. The emission was observed through a 450-nm cutoff filter (KV450, G. Schott, Mainz) and a Bausch and Lomb high-intensity monochromator with entrance and exit slits of 2.54 and 1.78 mm, respectively. The monochromator was driven in 1.34-nm steps by a stepping motor. At each wavelength, the intensity was calculated by integrating the averaged decay in a specified time window.

Both luminescence decay lifetimes and T-jump relaxation times, obtained by the above analysis as a function of DNA concentration, were fit to kinetic models on a UNIVAC 1108 computer. A modified version of the fitting program SIMFIT, written by Manfred Jung, based on the Simplex routine (Nelder & Mead, 1964) was employed to yield estimates for the kinetic parameters. Characteristic equations describing the eigenvalues were solved numerically for polynomials of order 3. For second-order equations, the expressions were solved analytically.

RESULTS

Temperature-Jump Kinetics of Poly[d(A-br^{5}U)]–Proflavin Complex. The solution fluorescence exhibited a rapid, unresolvable, small-intensity decrease after the temperature jump. This change, seen in the absence or presence of DNA, was previously noted by Ramstein et al. (1980) and attributed to the temperature dependence of the fluorophore quantum yield. It will not be considered further. At DNA concentrations <~50 μM, a "fast" increase of the fluorescence intensity with a relaxation time τ_{fast} was observed (Figure 1A). At DNA

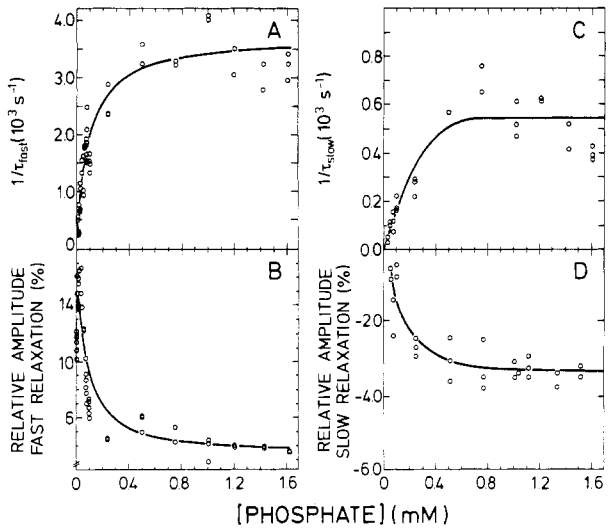

FIGURE 2: Inverse relaxation times and relative amplitudes for T-jump perturbations of proflavin complexes with poly[d(A-br^{5}U)]. Inverse of the fast (A) and slow (C) relaxation times and corresponding relative amplitudes (B) and (D), respectively, as a function of total poly[d(A-br^{5}U)] concentration. The solid lines passing through the points in (A) and (B) are theoretical fits according to the parallel and series model (see text) while those in (C) and (D) have no theoretical significance.

concentrations $>\sim 50$ μM, a much slower decrease of the fluorescence with a relaxation time τ_{slow} followed the fast relaxation mode (Figure 1B). The relaxation spectrum was best represented by the sum of two exponentials, as judged by the residuals. The variations of the individual relaxation times with total DNA concentration are plotted in Figure 2A,C, and the behavior for the corresponding amplitudes is plotted in Figure 2B,D. As previously mentioned, proflavin bleaches irreversibly upon irradation; the chromophore bleaches faster in the presence of poly[d(A-br^{5}U)] than when complexed to poly[d(A-T)]. However, photobleaching can be ruled out as a trivial explanation of the slower second process because control measurements done in the absence of a T-jump exhibited a constant fluorescence intensity for up to 750 ms. Cooling was also not responsible, since the fluorescence observed for measurements conducted with poly[d(A-T)] at DNA concentrations >1 mM reached a plateau following the initial increase, which remained constant for up to 100 ms.

$1/\tau_{fast}$ varies linearly with the DNA concentration initially and reaches a plateau at higher DNA concentrations; the corresponding relative amplitude has a maximum at ~ 10 μM nucleotides. The DNA concentration dependences of the relaxation time and amplitude for this faster process are similar to those of the single-mode relaxation spectrum observed by Ramstein et al. (1980) in T-jump studies of the poly[d(A-T)]–proflavin complex, which were repeated during the present investigation (data not shown). Such a concentration-dependent behavior is characteristic of a faster bimolecular step coupled to a slower kinetic process. Scheme I depicts two alternative models that account for this sequence of events. In Scheme I, C_e denotes a complex in which proflavin is externally bound to the double helix, C_{int} represents the intercalated proflavin complex, and the superscripts s and p refer to the series and parallel models, respectively. Ramstein and co-workers proposed only the former model to explain their results with poly[d(A-T)] and proflavin although, under the conditions of the T-jump measurements, the two models cannot be distinguished.

Reliable data for the slower relaxation mode were difficult to obtain between 50 and 100 μM DNA as the corresponding

Scheme I

Series Model

$$\text{DNA + Proflavin} \underset{}{\overset{K_e^s}{\rightleftharpoons}} C_e \underset{k_{-1}^s}{\overset{k_1^s}{\rightleftharpoons}} C_{int}$$

Parallel Model

$$\text{DNA + Proflavin} \overset{K_e^p}{\rightleftharpoons} C_e \qquad \text{DNA + Proflavin} \underset{k_{-1}^p}{\overset{k_1^p}{\rightleftharpoons}} C_{int}$$

amplitude became very small, and for <50 μM was undetectable. As a result, it was difficult to perform a complete analysis simultaneously incorporating both relaxation modes. The two relaxation times were well separated in time throughout the concentration range studied. If the assumption is made that the two modes are kinetically uncoupled, then as a first approximation, they can be treated separately. We will discuss first only the fast mode (τ_{fast}) and later the slower mode (τ_{slow}).

The reciprocal relaxation times describing the normal mode corresponding to intercalation coupled to the steady-state external binding equilibrium for both models, respectively, in Scheme I are given by

$$1/\tau_{fast}^s = k_1^s K_e^s [P_0]/(1 + K_e^s [P_0]) + k_{-1}^s \qquad (1a)$$

$$1/\tau_{fast}^p = k_1^p [P_0]/(1 + K_e^p [P_0]) + k_{-1}^p \qquad (1b)$$

in which $[P_0]$, the total DNA concentration, has been substituted for the free concentration [P] (valid for [P] $\gg$ [Pro], the latter being the concentration of unbound proflavin). Both expressions have the same mathematical form and, therefore, predict the same qualitative behavior for the intercalation data. A summary of the ground-state parameters obtained by fitting the reciprocal times in Figure 2A according to eq 1a and 1b is found in Table I. Also listed are the kinetic parameters for poly[d(A-T)] found by Ramstein et al. (1980). Normal-mode amplitude analyses of the relative relaxation amplitudes in the poly[d(A-br^{5}U)] T-jump series (Figure 2B) were performed. In both models of Scheme I, the two steps are independent and, judging from the widely separated relaxation times, kinetically uncoupled. Expressions for the relative amplitudes as a function of the kinetic parameters and $[P_0]$ were derived for both two-step models with the formalism developed by Jovin (1975) (Appendix A). The faster bimolecular step in each model of Scheme I predicts a relaxation time that increases linearly with $[P_0]$, a behavior that was not observed. If the forward rate were diffusion-controlled (i.e., $k \simeq 10^9$ M^{-1} s^{-1}), at 10 μM $[P_0]$ the relaxation time would be 10–100 μs assuming a dissociation rate of $\leq 10^5$ s^{-1}, a time detectable with the T-jump technique. Hence, the inital binding step is accompanied by no change in fluorescence ($\Delta F_e = 0$) and/or enthalpy ($\Delta H_e = 0$). As was done previously in the study of proflavin binding to poly[d(A-T)] (Ramstein et al., 1980), we assumed for the purpose of analysis that the first condition was operative. The values obtained for K_e, k_1, and k_{-1} in each model from the analysis of the $1/\tau_{fast}$ were substituted into the appropriate expression for the relative amplitude (eq A6), and a least-squares fit to the resulting expression was performed on the relative amplitude data. The enthalpies for both steps and normalized fluorescence factors for the second step of each model are included in Table I. As expected, the rate and amplitude analyses for the two different models yielded indistinguishable fitted curves. It can be seen in Figure 2B that the scatter in the amplitude data is rather large. This may be attributed to proflavin photobleaching, which causes changes in the chromophore concentration (i.e.,

Table I: Parameters of Proflavin Binding to Poly[d(A-T)] and Poly[d(A-br^{5}U)][a]

Series Model											
polymer	K_e^{*s} (10^4 M^{-1})[b]	K_e^s (10^4 M^{-1})[b]	k_1^{*s} (10^3 s^{-1})	k_1^s (10^3 s^{-1})	k_{-1}^{*s} (10^2 s^{-1})	k_{-1}^s (10^2 s^{-1})	k_{d1}^* (10^3 s^{-1})	k_{d2}^* (s^{-1})	k_{d3}^* (s^{-1})	$\Delta\Phi_1$	ΔH (kcal/mol)
poly[d(A-T)]											
excited state	4.2		0.81		2.5		3.4	6	65		
ground state		0.46 ± 0.15		3.6 ± 0.9		0.80 ± 0.1				−0.18 ± 0.04[c]	$\Delta H_e + \Delta H_1 = -4$
poly[d(A-br^{5}U)]											
excited state	100 (37–170)		0.11 (0.11–1.2)		1.6 (0.4–1.6)		4.3 (3.8–11)	450 (36–450)	120 (120–270)		
ground state		1.12 ± 0.02		3.6 ± 0.3		0.9 ± 0.5				−0.98 ± 0.1	$\Delta H_e = -6.5 \pm 0.7$
											$\Delta H_1 = -2.8 \pm 0.4$

Parallel Model											
polymer	K_e^{*p} (10^3 M^{-1})[b]	K_e^p (10^3 M^{-1})[b]	k_1^{*p} (10^7 M^{-1} s^{-1})	k_1^p (10^7 M^{-1} s^{-1})	k_{-1}^{*p} (10^2 s^{-1})	k_{-1}^p (10^2 s^{-1})	k_{d1}^* (10^3 s^{-1})	k_{d2}^* (s^{-1})	k_{d3}^* (s^{-1})	$\Delta\Phi_1$	ΔH (kcal/mol)
poly[d(A-T)][d]											
excited state											
ground state		6.7		16		0.9					
poly[d(A-br^{5}U)]											
excited state											
ground state		11.2 ± 0.4		4.1 ± 1.3		0.9 ± 0.8				−0.98 ± 0.1	$\Delta H_e = -6.5 \pm 0.6$
											$\Delta H_1 = -9.3 \pm 0.7$

[a] The ground-state parameters for poly[d(A-T)] were determined at 17 °C and were taken from Table I of Ramstein et al. (1980) while those for poly[d(A-br^{5}U)] were determined in this work at 13.9 °C and are given with the estimated standard deviations. The excited-state parameters for poly[d(A-br^{5}U)] are reported for a representative experiment. The ranges of values in parentheses were determined from several experiments and are biased by extreme results from individual cases. Only one experiment was performed for poly[d(A-T)]. The asterisk (*) denotes excited-state parameters determined from delayed fluorescence decay measurements conducted at 24 °C. All other parameters were obtained from temperature-jump data. [b] Superscripts s and p refer to the series model of Scheme I and the parallel model with $n = 2$ (Appendix A), respectively. K's and k's are the corresponding equilibrium and kinetic rate constants. Values of $\Delta\Phi_1$, the fractional change in fluorescence normalized to the fluorescence of unbound proflavin, were determined for poly[d(A-br^{5}U)] by amplitude analysis of temperature-jump data. [c] Estimated from data presented in Table I of Ramstein et al. (1980) assuming $\epsilon_{436} = 3.87 \times 10^3$ M^{-1} cm^{-1} and a fluorescence quantum yield of 0.39 for unbound proflavin. [d] Estimates of the ground-state constants for the parallel model were made from data presented in Figure 3 of Ramstein et al. (1980).

total fluorescence), despite the precautions taken. The rates are little affected as $[P_0] \gg [Pro]$; however, the expressions for the relative amplitudes are strongly dependent on the absolute proflavin concentration. For this reason, experiments were repeated at each temperature at least twice and more often at lower DNA concentrations for which the amplitudes changed more rapidly. The same forward and reverse rate constants for the proposed intercalation step are found for both polymers. K_e for poly[d(A-br^{5}U)] is a factor of ~ 2 greater than that for poly[d(A-T)], indicating that the former polynucleotide has a somewhat higher affinity for proflavin. Clearly, a mechanism more complicated than Scheme I is required to describe the total T-jump relaxation spectrum of the poly[d(A-br^{5}U)]–proflavin complex (see Discussion).

Fluorescence Titration. The fluorescence is partially quenched upon titration of proflavin with poly[d(A-br^{5}U)]. If one assumes the two-step series binding process of Scheme I, then the overall binding constant for the reaction, $K_a = K_e^s(1 + K_1^s)$, where $K_1^s = k_1^s/k_{-1}^s$ (Table I), can be estimated from the fluorescence titration. The conditions of the titration were chosen such that the concentration of free binding sites was always in great excess over bound dye. A plot of $1/[(F/F_0) - 1]$ vs. the reciprocal DNA concentration $1/[P_0]$ according to

$$1/[(F/F_0) - 1] = \{K_e^s[\Delta\Phi_e^s + (\Delta\Phi_1^s + \Delta\Phi_e^s)K_1^s]\}^{-1}\{(1/[P_0]) + K_a\} \quad (2)$$

gives a straight line with the slope $= 1/\{K_e^s[\Delta\Phi_e + (\Delta\Phi_1 + \Delta\Phi_e)K_1^s]\}$ and the intercept = slope $\times K_a$. F and F_0 are the fluorescence intensities of proflavin in the presence and absence of DNA, respectively. $\Delta\Phi_e$ and $\Delta\Phi_1$ are the relative changes in proflavin fluorescence observed for the first and second steps, respectively, of the mechanisms shown in Scheme I (see also Appendix A). $\Delta\Phi_e$ was assumed to equal zero for analyses of the T-jump amplitude data (see above). A $K_a = 1.5 \times 10^5$ M^{-1} was obtained from a plot according to eq 2 (data not shown) and can be compared to the overall equilibrium constants of $(2.7–11) \times 10^5$ M^{-1} calculated from the T-jump data in Table I according to the series model and with the most extreme combinations of mean values and standard deviations. For $\Delta\Phi_e = 0$ and $K_1^s \gg 1$, the intercept becomes $1/\Delta\Phi_1$. A value of -2.2 extrapolated from the plot yields $\Delta\Phi_1 \simeq -0.45$ in comparison to a value of -0.98 (Table I) from the T-jump analysis. The magnitude of $\Delta\Phi_1$ is the fractional quenching experienced by the dye upon intercalation, i.e., 0.45 and 0.98 for the two methods, respectively.

Delayed Fluorescence Kinetics. Typical curves for the delayed fluorescence decay $S(t)$ of proflavin bound to poly[d(A-T)] and poly[d(A-br^{5}U)] are shown in Figure 3 (A and C). Superposed are the fits to sums of two exponentials according to

$$S(t) = \alpha_1 e^{-t/\tau_1} + \alpha_2 e^{-t/\tau_2} \quad (3)$$

in which τ_1 and τ_2 denote the two analyzed lifetimes. A weighted residuals plot (insets of the same figures) and an expansion (Figure 3B,D) of each of these curves, respectively, show that a two exponential analysis is sufficient to describe the decay for both polymers.

The delayed luminescence spectra of both DNA–proflavin complexes show apparent maxima at ~ 500 nm (Figure 4), which are similar to those of the prompt fluorescence spectra of 0.1 μM proflavin (data not shown). In ethanol at -70 °C, the proflavin fluorescence has a maximum at 492 nm (Parker et al., 1964) while the delayed emission spectrum at this low temperature reveals maxima at 492 nm (delayed fluorescence) and at 582 nm (phosphorescence). By analogy, the delayed

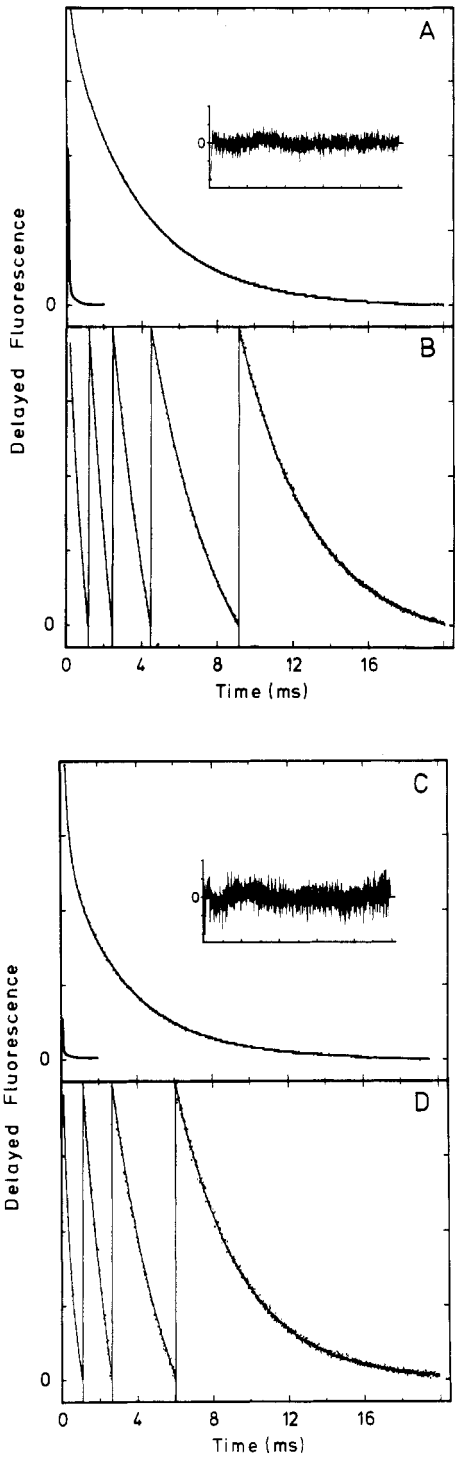

FIGURE 3: Total decay of the delayed luminescence for proflavin alone and complexed to DNA: (A and B) poly[d(A-T)] and (C and D) poly[d(A-br^{5}U)] at 23 °C. The solid curves in the lower left-hand corner of (A) and (C) represent fits of the delayed fluorescence decay of proflavin alone in solution ($\tau = 292$ μs). The larger curves in (A) and (C) are the total decay of DNA–dye complex delayed fluorescence and the superimposed fits to a weighted biexponential analysis. The insets are the residuals plot, the corresponding ordinates of which are on a scale 50 times that of the decay curves. The steplike nature of these and subsequent plots results from the limited resolution of the computer graphics unit employed. (B and D) Division of the proflavin–DNA curves in (A) and (C), respectively, along the time axis with an ordinate expansion of the curve for each section. Solution conditions: proflavin 0.1 μM; poly[d(A-T)] 50 μM; poly[d(A-br^{5}U)] 95 μM. For (A) and (B), the observed lifetimes are $\tau_1 = 0.58$ ms and $\tau_2 = 4.93$ ms, and for (C) and (D), $\tau_1 = 0.33$ ms and $\tau_2 = 3.36$ ms. $\lambda_{obsd} > 550$ nm.

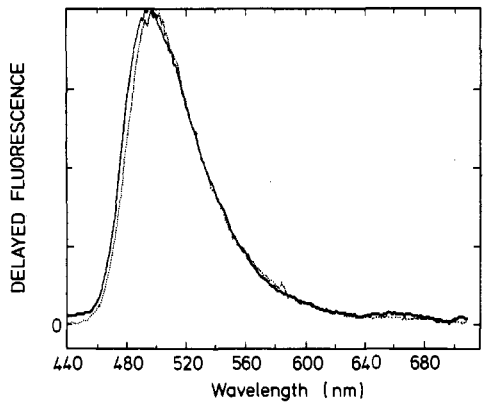

FIGURE 4: Time-resolved delayed fluorescence spectra (uncorrected) to proflavin complexed with DNA: Poly[d(A-T)] (—) 94 μM, and proflavin 0.094 μM; poly[d(A-br^{5}U)] (...) 10 μM, proflavin 0.1 μM, integration was conducted over the time window 0.48–9.84 ms. The ordinate axes are scaled in arbitrary units.

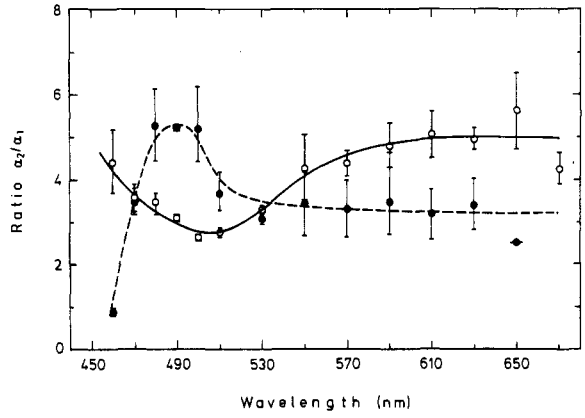

FIGURE 5: Spectrally resolved amplitude ratios for two components of delayed proflavin–DNA luminescence. Solution conditions: 50 μM DNA and 0.1 μM proflavin. (○) Poly[d(A-br^{5}U)]; (●) poly-[d(A-T)]. λ_{ex} = 415 nm. Each point represents the average determination of two experiments, and the error bars show the range spanned by the two measurements. Emission was observed through narrow band-pass filters centered at the wavelengths indicated.

luminescence observed in our measurements is identified as delayed fluorescence. Comparison of this emission from free proflavin (Figure 3A,C) with the signals corresponding to the two DNA–dye solutions demonstrates the large increase in total delayed fluorescence yield and lengthening of the decay times upon formation of complexes. This effect was observed with another poly[d(A-T)] analogue, poly[d(A-i^{5}U)] (data not shown), but was not seen with poly[d(G-C)], poly[d(G-br^{5}C)], and poly[d(G-m^{5}C)]. This is not surprising as it is known that the fluorescence of proflavin is quenched when bound to poly[d(G-C)] (Φ = 0.05, compared to the free dye, Φ = 0.7) and slightly enhanced when bound to poly[d(A-T)] (Φ = 0.74) (Pachmann & Rigler, 1972). Hence, because the delayed luminescence is fluorescence, the G-C family would be expected to quench the delayed emission below a level detectable in our system.

The spectral distribution of the amplitudes resulting from a biexponential analysis for both polymers complexed to proflavin was collected by using narrow band-pass filters between 460 and 650 nm. At each wavelength, the decay curve obtained was analyzed as usual and the ratio of the amplitudes α_2/α_1 plotted as a function of the center wavelength of the band-pass filter (Figure 5). The ratio shows a maximum at ~490 nm for poly[d(A-T)] and a minimum at ~510 nm for poly[d(A-br^{5}U)], thus providing further evidence that multiple excited triplet species of proflavin exist in the presence of the

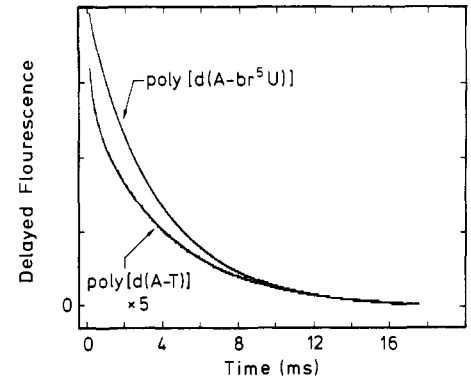

FIGURE 6: Heavy atom effect on the delayed emission of proflavin bound to poly[d(A-br^{5}U)] vs. poly[d(A-T)]. Total decay of the delayed fluorescence emission. Both DNA polymers were present at 50 μM and, proflavin was at 0.1 μM. The curve corresponding to poly[d-(A-T)] has been vertically expanded 5 times along the ordinate, which is scaled in arbitrary units.

DNA and that they contribute with different weights to the two normal relaxation modes. The different nature of the two extrema is most probably related to specific proflavin–bromine atom interactions, which necessarily pertain only to the substituted polymer.

When proflavin was complexed with the halogenated analogues of poly[d(A-T)], the yields of delayed fluorescence were enhanced and the lifetimes shortened such that the values increase in the order poly[d(A-i^{5}U)] (data not shown) < poly[d(A-br^{5}U)] < poly[d(A-T)], a result indicative of an external heavy atom effect. A comparison of the delayed emission exhibited by the polymers is given in Figure 6.

A treatment of excited state ligand binding processes has been presented by Rigler and Ehrenberg (1973). According to the formalism given by these authors, dynamic binding of proflavin in the excited state should be coupled in time to the delayed fluorescence if the excited-state binding rates are comparable to the delayed luminescence decay rates. In this case, the luminescence decay lifetimes observed ($\lambda_i = 1/\tau_i$) are the eigenvalues obtained in a normal-mode analysis of the differential equations including the coupling. These λ_i's are functions of [P_0], the excited-state chemical rate constants, and the photophysical decay rate constants. The two observed reciprocal decay lifetimes ($1/\tau_1$ and $1/\tau_2$), as determined in a biexponential analysis of the decay of the total delayed fluorescence, are plotted vs. the total DNA concentration in Figure 7. Both exhibit a dependence on the DNA concentration, thereby establishing the coupling between the chemical and photophysical relaxation kinetics. The decay rates decrease (lifetimes increase) with increasing DNA concentration. The lifetime of proflavin alone in buffer was determined to be 280 μs, whereas the longest times found for the complexes to poly[d(A-br^{5}U)] and poly[d(A-T)] were 4.5 and 15 ms, respectively.

The following procedure was adopted in searching for a mechanism that incorporates both the excited-state dynamic equilibrium and the luminescence decay processes. With Scheme I as a starting point, necessary additional complexities were added, and the resulting mechanism was simulated by employing a relaxation kinetics simulation program written by Avery (1982). In this manner, a minimal mechanism (Scheme II) was found that could adequately describe the plots of reciprocal luminescence decay rates as a function of total DNA concentration for both polymers. Scheme II incorporates the dynamic binding steps of proflavin in the excited triplet state (top row) and ground state (bottom row). The relaxation processes from the excited triplet state back to the ground state

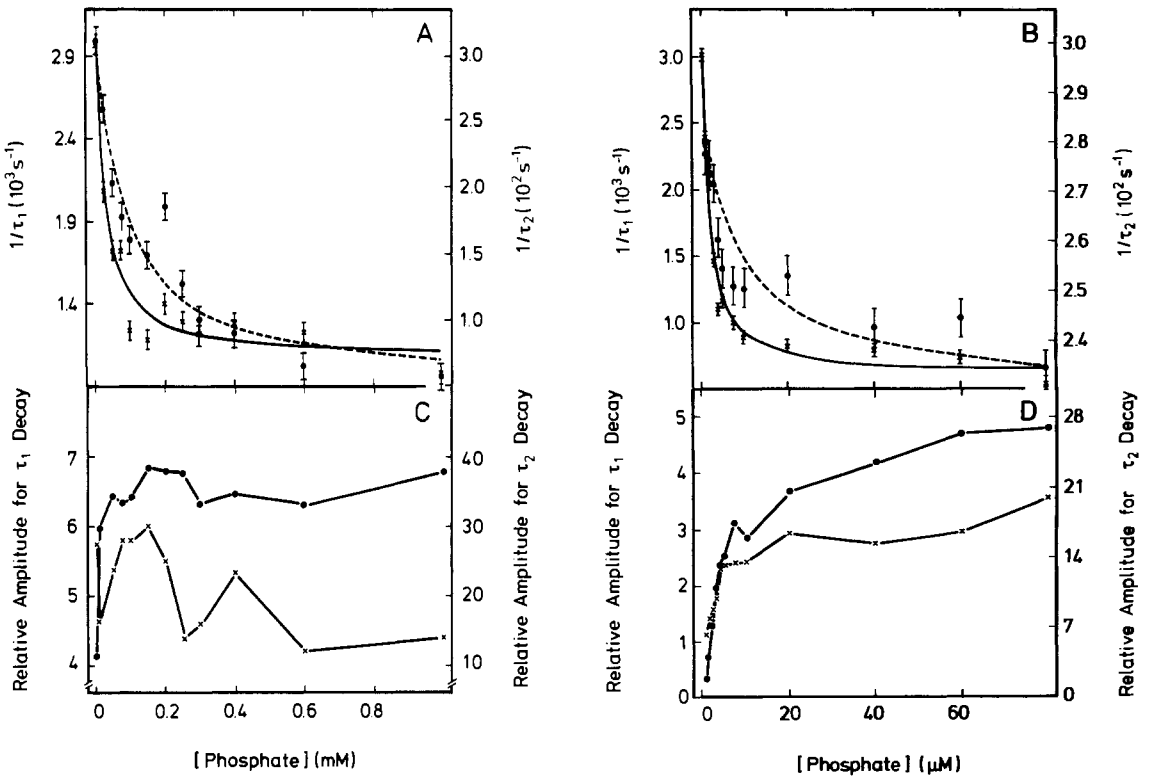

FIGURE 7: Dependence of the reciprocal times and amplitudes for proflavin luminescence on DNA concentration. (A and B) Reciprocal times and (C and D) corresponding relative amplitudes resulting from a biexponential analysis of the decay curves. (A and C) Poly[d(A-T)]; (B and D) poly[d(A-br^{5}U)]. Proflavin was at 0.1 μM throughout. The error bars represent the normalized standard deviation of the complete data set as reported by the fitting program and reflect the statistical scatter in the data. The solid (—) and dashed (– –) lines are the computer fits to the reciprocal times $1/\tau_1$ (×) and $1/\tau_2$ (●), respectively.

Scheme II

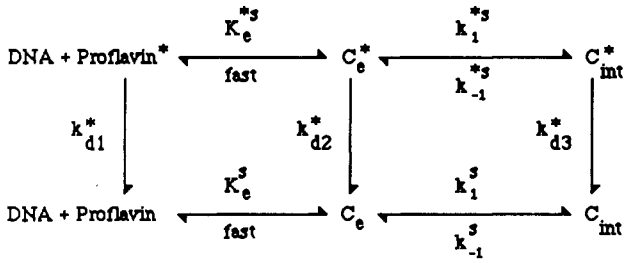

in Scheme II are fully characterized by seven parameters if all the forward, k_i^{*s}, and reverse, k_{-i}^{*s}, chemical kinetic rate constants and the three photophysical decay rate constants, k_{di}^*, are considered. The latter contain the rates for thermal activation from the triplet state to the first excited singlet state and emission from this state. [Not indicated are the initial "delta" excitation processes, which generate the triplet population. They proceed during the actinic flash of ~10-ns duration, i.e., in a time shorter than the 120 μs discarded in the analysis (see Methods).] The three differential equations describing the change in time of the excited-state species leads to a 3 × 3 rate matrix (shown in Appendix C), which predicts three eigenvalues corresponding to the normal modes of delayed fluorescence emission decay coupled to the chemical kinetic reequilibration of triplet-state dye species. Simulation shows that the fastest mode, $1/\tau_1^{sim}$ (the superscript denotes simulation), largely reflects the initial bimolecular binding process which increases linearly as a function of $[P_0]$. For a certain range of parameter values, the two slower reciprocal times, $1/\tau_2^{sim}$ and $1/\tau_3^{sim}$, are seen to decrease as a function of $[P_0]$ (Figure 8). As discussed under Methods, our spectrometer has an effective deadtime of ~120 μs resulting from the very large prompt fluorescence exhibited by proflavin; hence, $1/\tau_1^{sim}$ might not be detectable if the initial binding step is very fast, i.e., diffusion controlled. Therefore, the forward (k_e^{*s}) and reverse (k_{-e}^{*s}) rate constants cannot be determined explicitly. Assuming a fast equilibrium process for the first step reduces the number of differential equations to two, or equivalently to the 2 × 2 rate matrix of Appendix C, which predicts two relaxation times. Analysis of the two observed decay processes in terms of this simpler mechanism yields the ratio $K_e^{*s} = k_e^{*s}/k_{-e}^{*s}$, reducing the parameter count to six. The reciprocals of the two experimentally observed decay times behave in a manner similar to that of the simulated inverse times, $1/\tau_2^{sim}$ and $1/\tau_3^{sim}$.

Estimates for the six excited-state parameters in Scheme II were initially obtained by simulation in which the full set of seven parameters was actually employed. This was accomplished by systematically varying the values of the chemical kinetic and emission decay constants and comparing plots of the simulated modes, $1/\tau_2^{sim}$ and $1/\tau_3^{sim}$, with plots of the experimental data. This procedure offers three advantages: (1) the range of reasonable parameter values yielding a good simulation can be visually assessed; such values provide good initial estimates for subsequent fitting procedures; (2) the uniqueness of a given parameter can be quickly evaluated; (3) the subroutine logic, in the fitting program, for a given mechanism and the "ability" of the fitting program to find the correct parameters can be checked by fitting known simulated curves. A demonstration of these points follows.

Although the number of parameters is large, simulations show that the range of values is restricted by various features of the plots. For example, the normal modes (eigenvalues) $1/\tau_2^{sim}$ and $1/\tau_3^{sim}$ of Scheme II decrease as a function of increasing $[P_0]$ only for a narrow range of K_e^* values. Analogously, the ordinate intercepts for these two eigenvalues (i.e., where $[P_0]$ approaches 0) limit the possible values of k_{d1}^* to

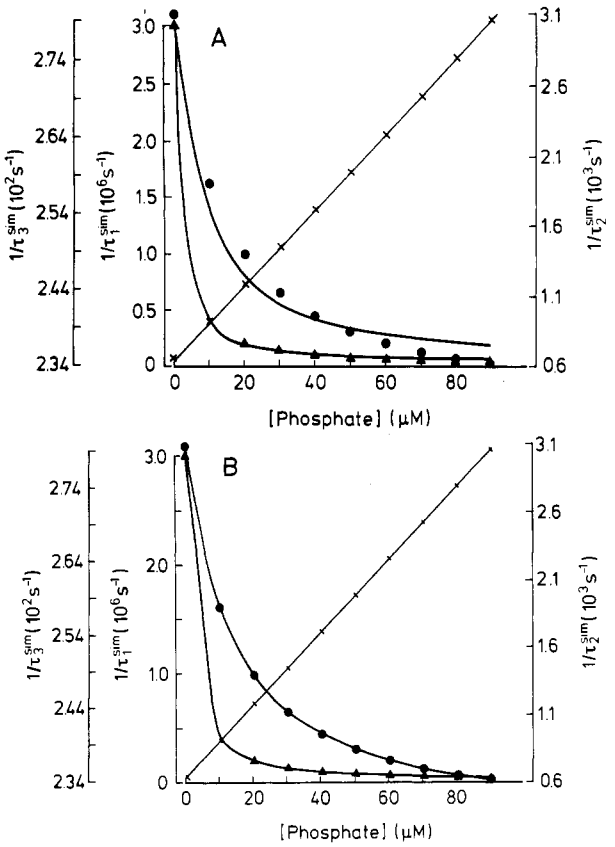

FIGURE 8: Simulations of the reciprocal luminescence lifetimes as a function of DNA concentration as predicted by Scheme II for the excited-state processes. The solid lines represent the fits generated by providing the analysis program with (A) kinetic parameter estimates greater than a factor of 10 different from the correct values used for the simulation and (B) the parameters found at convergence of the fit in (A). The parameters are $k^*_{d1} = 3.78 \times 10^3\ s^{-1}$, $k^*_{d2} = 2.92 \times 10^2\ s^{-1}$, $k^*_{d3} = 2.12 \times 10^2\ s^{-1}$, $k^{*s}_e = 3.33 \times 10^{10}\ M^{-1}\ s^{-1}$, $k^{*s}_{-e} = 3.63 \times 10^3\ s^{-1}$, $k^{*s}_1 = 2.4 \times 10^2\ s^{-1}$, and $k^{*s}_{-1} = 74.3\ s^{-1}$, where $k^{*s}_e/k^{*s}_{-e} = K^{*s}_e$ (see text for discussion). The computer-simulated rates $1/\tau_1^{sim}$, $1/\tau_2^{sim}$, and $1/\tau_3^{sim}$ are represented by (×), (△), and (●), respectively.

a narrow range. Hence, good simulations can only be achieved for values of k^*_{d1} and K^*_e that vary less than a factor of 2 from the fitted values in Table I. The values of other parameters are less critical for obtaining a good simulation. For example, k^*_{d2} and k^*_{d3} can vary by a factor of 10 from the values given in Table I. In general, the somewhat independent limitations on the range of possible parameter values suggest that a reduced parameter space can be searched in a least-squares fit of the experimental data to the model. As a test, the simulated data set of Figure 8 were fit with a nonlinear least-squares fitting program. The correct values of the parameters used in generating the data were not found when initial parameter estimates were greater than a factor of 10 from the correct answer. If, however, the values obtained from the first fitting attempt were entered as initial estimates for a refit, the correct parameters were obtained.

Estimates for chemical kinetic and decay parameters resulting from a least-squares fit of the triplet-state decay measurements conducted for both DNAs investigated are summarized in Table I. The same overall series chemical kinetic scheme employed in analysis of the ground-state data was sufficient to describe the excited-state kinetics of proflavin binding. The fitted values of the chemical kinetic constants and two of the emission decay rate constants are, however, quite different for the two polymers. As discussed above in connection with simulations, all parameters were not equally well determined (see ranges listed in Table I). For poly[d-(A-br^{5}U)], the initial binding event characterized by K^{*s}_e is ~24 times larger than that for poly[d(A-T)], while the intercalation step, as characterized by k^{*s}_1/k^{*s}_{-1} ($=K^*_1$), is more favorable for the unsubstituted polymer ($K^*_1 \simeq 3$) than for the bromine-substituted helix ($K^*_1 \simeq 0.7$). The overall binding constants of proflavin in the excited triplet state bound to poly[d(A-T)] and poly[d(A-br^{5}U)], given by $K^{*s}_a = K^{*s}_e(1 + K^{*s}_1)$, are $\sim 1.8 \times 10^5$ and 1.7×10^6, respectively, indicating a much tighter binding to the latter polymer.

A similar analysis was attempted for the triplet data in which a parallel kinetic model was employed for the excited-state chemical kinetics. In this model, a fast bimolecular outside binding step is coupled to a second, slower, direct bimolecular intercalation step. No satisfactory simulations could be found.

Discussion

Comparison of the Ground- and Excited-State Kinetics. Ground-state studies on the binding of the intercalating dye proflavin to poly[d(A-T)] and the halogenated analogue poly[d(A-br^{5}U)] show the similarity of the binding process for these two systems. A photophysical/chemical kinetic analysis of the total delayed fluorescence emission of both complexes reveals that in the excited state proflavin binds more strongly to the halogenated polymer. Analysis according to a series reaction mechanism yields a preliminary association step that is much stronger when proflavin is in the excited state than in the ground state. K^{*s}_e is ~10 times K^s_e for poly[d(A-T)] and ~100 times K^s_e for poly[d(A-br^{5}U)]. However, intercalation is less favorable for the dye in the excited state in comparison to the ground-state species by a factor of ~15 for poly[d(A-T)] and 40 for poly[d(A-br^{5}U)]. If the chromophore has approximately the same molecular structure in the triplet and ground states, these measurements attest to the importance of the electronic structure in determining binding characteristics.

The ground-state kinetic studies do not permit the distinction between the two-step series model and the two-step parallel mechanisms. In the former, a bimolecular binding step is followed by a monomolecular intercalation step. In the latter case, intercalation proceeds via a direct bimolecular step. The excited-state data, however, were found to be consistent only with a series model. This implies that the fundamental molecular events operating for binding of proflavin to DNA are the same for the ground and excited states. That is, intercalation in both cases is preceded by a general electrostatic association of the positively charged chromophore with the polyanionic DNA.

It remains to be established whether delayed fluorescence, in general, provides a means of distinguishing between parallel and series models, each entailing very different events on the molecular level. We recognize that the inability to simulate or fit data adequately does not conclusively eliminate a mechanism as it is very difficult to conduct a complete search of the entire parameter space.

Closer Inspection of τ_{slow}. The DNA concentration dependence of the slower relaxation time observed in the T-jump data of proflavin binding to poly[d(A-br^{5}U)] permits one to rigorously exclude a number of mechanisms. Two such reaction schemes are an "extended" parallel (i.e., $n \geq 3$) and an "extended" series model (i.e., $n \geq 3$) (see Appendix A). Clegg (1984) demonstrated that, in general, both predict a set of relaxations characterized by the relaxation times τ_i having the following properties: (1) a plot of $1/\tau_1$, corresponding to the fastest (bimolecular) reaction, increases linearly as the sum of the equilibrium concentrations of the reactants, $\bar{A} + \bar{B}$; all

other reciprocal times are monotonically increasing functions of $\bar{A} + \bar{B}$, which reach a plateau at larger reactant concentrations; (2) for $1/\tau_i > 1/\tau_{i+1}$, the intercept value (i.e., $\bar{A} + \bar{B} \rightarrow 0$) of $1/\tau_i$ is greater than the plateau value of $1/\tau_{i+1}$. Condition 1 is not observed for the binding of proflavin to poly[d(A-br^{5}U)] for reasons already mentioned. However, if the values of $1/\tau_{slow}$ at higher DNA concentrations (e.g., >800 μM) are considered to define a plateau (estimated by the solid curve drawn in Figure 2C), then the intercept of $1/\tau_{fast}$ is seen to be less than this plateau value, rigorously eliminating the two models above. Similar arguments can be employed to discount the branched series model for $n \geq 2$ defined in Appendix B. Attributing τ_{slow} to the slow exchange between two DNA conformational states, "active" and "inactive" with respect to proflavin binding, can also be discounted. At higher [DNA], more complex would be formed, thereby lowering the concentration of the free proflavin. Such a model predicts a decrease in the absolute amplitude corresponding to τ_{slow}, contrary to what is observed (Figure 2D).

The second, slower relaxation time at higher concentrations of DNA might be explained by more involved reaction schemes, involving DNA–DNA interactions (e.g., DNA-mediated interhelix ligand transfer; Ryan & Crothers, 1984), dye-mediated interhelix cross-linking (Neidle & Berman, 1983), and/or multiple binding sites along the helix having different quantum yields. Unfortunately, the quality of the data does not permit a quantitative analysis of these expanded mechanisms. DNA aggregation has been previously reported for B-DNA structures in solution: e.g., plasmid DNA in the presence of divalent cations (Post & Zimm, 1982) or multivalent cations (Widom & Baldwin, 1983) or solutions of poly[d(G-C)] containing divalent cations and ethanol (van de Sande & Jovin, 1982). However, there are no reports of such phenomena occurring with halogen-substituted polymers under our solution conditions.

Without a complete analysis, the overall binding constant as determined by T-jump data is inaccurate to the extent to which additional steps responsible for τ_{slow} play a significant role. K_a^s as determined by T-jump data is 2–11 times larger than that determined by fluorescence titration. We also note that the slower relaxation time was not detected in the triplet state.

Heavy Atom Effect. The two determinations of the decay rate of delayed fluorescence of unbound proflavin in solution (k_{d1}^*), from the model analysis of both DNA–dye complexes, are within a factor of ~1.25 and agree well with the reciprocal lifetime determined for proflavin alone in solution (3570 s^{-1}). The delayed fluorescence decay rate constants for both the outside bound and the intercalated dye species (k_{d2}^* and k_{d3}^*) are greater for the brominated polymer. Furthermore, the quenching of prompt fluorescence upon binding of proflavin to poly[d(A-br^{5}U] and the greater intensities of delayed emission are consistent with an ehancement of intersystem crossing. All these effects indicate that an external heavy atom effect is operative (Parker, 1968) as was inferred previously in studies by Galley and Purkey (1972) of the binding of proflavin to poly[d(A-br^{5}U] at 77 K. The latter authors experimentally determined the short range of ~4.5 Å over which the heavy atom effect operates, implying that the halogen atom and the bound drug species giving rise to the enhanced delayed fluorescence are in close proximity. The model they proposed involves two bound proflavin species, a partially intercalated heavy atom perturbed proflavin and a fully intercalated species that lies >4.5 Å away from the bromine atom. However, the model is based on assumptions about the geometric arrangement of the proflavin–poly[d(A-T)] complex for which there are no crystallographic data. The kinetic analysis reported in the present study suggests that both species may approach within the critical distance from the bromine atom. However, as the relevant luminescence decay constants are not well determined, conclusions based on small differences between them are speculative. Unequivocal is the fact that the emission rate constants for all DNA-bound forms of proflavin are much lower than those for the free drug in solution, suggesting that the excited triplet state is more protected from deactivation when bound to DNA.

The large increase in the equilibrium constant for the initial association step upon excitation of the dye (i.e., 1 and 2 orders of magnitude for poly[d(A-T)] and poly[d(A-br^{5}U)], respectively) implies that the heavy atom substituent has a significant structural effect on the helix, one that presumably is exerted also the ground state, and that external binding is inherently enhanced as a result of interaction with the triplet-state proflavin.

In conclusion, if the chemical, kinetic, and photophysical criteria outlined by Rigler and Ehrenberg (1973) are met, then the kinetics of any dynamic ligand–substrate binding process can be studied by measuring the luminescence decay times of ligand or substrate as a function of reactant concentrations. Thus, photophysical perturbation techniques offer an alternative to the kinetic methods based upon single or periodic shifts in thermodynamic variables such as temperature [Marcandalli et al., 1984; this study avoided the inherent problems associated with electric field discharges (Dourlent & Hogrel, 1976) by using infrared laser heating] and pressure (Macgregor et al., 1985; Marcandalli et al., 1986). We exploited the photophysical properties of the excited state. However, if one uses sufficient light energy so as to achieve a significant depletion of the ground state, the chemical kinetics of the latter can be investigated by monitoring prompt fluorescence with a second continuous light source. The adaptation of our instruments for such "fluorescence-depletion" (Johnson & Garland, 1981; 1982) experiments is described elsewhere (Corin et al., 1986).

ACKNOWLEDGMENTS

We are thankful to Reinhard Klement for technical assistance with computer analyses, Dr. Horst Ruf for facilitating the T-jump measurements, Dr. Robert Clegg for assistance with the derivation of Appendix B and critical reading of the manuscript, and Dr. Robert Macgregor for critical reading of the manuscript.

APPENDIX

(A) We consider the parallel and series models using the nomenclature of Clegg (1984):

parallel model

$$A + B \leftrightarrow C_1,\ A + B \leftrightarrow C_2,\ \ldots,\ A + B \leftrightarrow C_n \qquad \text{(A1a)}$$

series model

$$A + B \leftrightarrow C_1 \leftrightarrow C_2 \ldots C_{n-1} \leftrightarrow C_n \qquad \text{(A1b)}$$

For consistency with the main text, all terms referring to reactions $n = 1$ and 2 will be referred to with the subscripts e and 1, respectively. The absence of the superscripts s and p means that the expression is valid for both models.

To calculate the times and amplitudes of both models, in the case of two-step mechanisms, one solves the two linearized rate equations (Eigen & DeMaeyer, 1974; Guillain & Thusius, 1970). The relaxation times are the eigenvalues of the $\mathbf{r}\cdot\mathbf{g}$ matrix, where $\mathbf{r}$ is the diagonal square matrix of the reaction

step exchange rates and **g** is the symmetric square matrix relating the reaction free energies to the reaction advancements (Eigen & DeMaeyer, 1974; Castellan, 1963):

series model	parallel model
$g_{ee} = 1/[A] + 1/[B] + 1/[C_1]$	$g_{ee} = 1/[A] + 1/[B] + 1/[C_1]$
$g_{e1} = g_{1e} = -1/[C_1]$	$g_{e1} = g_{1e} = 1/[A] + 1/[B]$
$g_{11} = 1/[C_1] + 1/[C_2]$	$g_{11} = 1/[A] + 1/[B] + 1/[C_2]$

(A2)

The amplitudes are derived by combinations of the same matrices (Jovin, 1975; Thusius, 1977). In the case that the first step of each of the models above (characterized by the equilibrium constant K_e) is fast and kinetically uncoupled from the second step, Jovin (1975) has shown that the general expression for the signal change associated with the second step of both mechanisms is given by

$$\Delta P_1 = [g_{ee}/(g_{ee}g_{11} - g_{e1}^2)][-(g_{e1}/g_{ee})\Delta F_e + \Delta F_1] \times [-(g_{e1}/g_{ee})\Delta H_e + \Delta H_1](\Delta T)/(RT^2) \quad \text{(A3)}$$

ΔF_e and ΔF_1 are the specific fluorescence signal changes and ΔH_e and ΔH_1 the changes in enthalpy corresponding to steps 1 and 2, respectively. The total fluorescence can be written as

$$F = [B]f_B + [C_1]f_{C_1} + [C_2]f_{C_2} \quad \text{(A4)}$$

where f_i (i = B, C_1, C_2) is the fluorescence signal per unit concentration of species i under the instrumental conditions of excitation and detection of emission. Species A has no detectable fluorescence at the monitoring wavelength (i.e., $f_A = 0$).

The specific fluorescence signal changes are $\Delta F_e^s = f_{C_1} - f_B$ and $\Delta F_1^s = f_{C_2} - f_{C_1}$ for the series model and $\Delta F_e^p = f_{C_1} - f_B$ and $\Delta F_1^p = f_{C_2} - f_B$ for the parallel model. Substituting these into eq A4 yields specific expressions for the total solution fluorescence:

$$F^s = [B]f_B\{1 + [A]K_e^s\{(1 + \Delta\Phi_e^s) + K_1^s(1 + \Delta\Phi_e^s + \Delta\Phi_1^s)\}\}$$
$$F^p = [B]f_B\{1 + [A]\{K_e^p(1 + \Delta\Phi_e^p) + K_1^p(1 + \Delta\Phi_1^p)\}\} \quad \text{(A5)}$$

The K's are the equilibrium constants of Scheme I. $\Delta\Phi_e^s = \Delta F_e^s/f_B$ and $\Delta\Phi_e^p = \Delta F_e^p/f_B$, and analogously, $\Delta\Phi_1^s = \Delta F_1^s/f_B$ and $\Delta\Phi_1^p = \Delta F_1^p/f_B$. If no fluorescence change accompanies the first step, then $f_{C_1} = f_B$; i.e., $\Delta F_e = 0$.

Assuming that the change in f_B is small over the temperature jumped, factoring out this term from eq A3 and normalizing by the total solution fluorescence F gives the relative amplitude of the second normal mode:

$$\Delta P'_1 = \Delta P_1/F = \{[g_{ee}/(g_{ee}g_{11} - g_{e1}^2)](\Delta\Phi_1) \times [-(g_{e1}/g_{ee})\Delta H_e + \Delta H_1]\}\{(\Delta T)/(RT^2)\}f_B/F \quad \text{(A6)}$$

To obtain the specific expressions for each model, one needs to substitute the corresponding terms F and $\Delta\Phi_1$ with the appropriate superscripts (s or p).

(B) Qualitative general characteristics are derived for the branched series kinetic model in a manner analogous to that employed by Clegg (1984) for the parallel and series kinetic models:

branched series model

$$A + B \underset{k_{-1}^b}{\overset{k_1^b}{\leftrightarrow}} C;\ C \underset{k_{-2}^b}{\overset{k_2^b}{\leftrightarrow}} D_1;\ C \underset{k_{-3}^b}{\overset{k_3^b}{\leftrightarrow}} D_2;\ ...;\ C \underset{k_{-(n+1)}^b}{\overset{k_{(n+1)}^b}{\leftrightarrow}} D_n \quad \text{(B1)}$$

According to Castellan (1963), the linear differential equations defining the branched model can be defined in terms of the extents of the reactions $\Delta\epsilon_i$, where i represents the ith reaction step. $\Delta\epsilon_i = \epsilon_i - \epsilon_i^0$, ϵ_i = extent of the ith reaction during the relaxation, and ϵ_i^0 = extent of the ith reaction at equilibrium after the perturbation; ϵ_i varies from 0 to 1. The matrix differential equations for the branched series model are then

$$-d/dt\{\Delta\boldsymbol{\epsilon}_b\} = \begin{bmatrix} k_1a_1+k_{-1} & -k_{-1} & -k_{-1} & -k_{-1} & \dots & -k_{-1} \\ -k_2 & k_2+k_{-2} & k_2 & k_2 & \dots & k_2 \\ -k_3 & k_3 & k_3+k_{-3} & k_3 & \dots & k_3 \\ -k_4 & k_4 & k_4 & k_4+k_{-4} & \dots & k_4 \\ \dots & \dots & \dots & \dots & \dots & \dots \\ \dots & \dots & \dots & \dots & \dots & \dots \\ \dots & \dots & \dots & \dots & \dots & \dots \\ -k_n & k_n & \dots & \dots & \dots & k_n+k_{-n} \end{bmatrix} \Delta\boldsymbol{\epsilon}_b \quad \text{(B2)}$$

where $\Delta\epsilon_b$ represents the column vector ($\Delta\epsilon_1$, $\Delta\epsilon_2$, $\Delta\epsilon_3$, ...) and $a_1 = (\bar{A} + \bar{B})$, the sum of the equilibrium concentrations of A and B. The superscript b, on all kinetic parameters, has been dropped for clarity. The characteristic equation resulting from expansion of the eigenvalue determinant is

$$[k_1(a_1) + k_{-1} - \lambda]\prod_{j=2}^{n}(k_{-j} - \lambda) + [k_1(a_1) - \lambda]\sum_{j=2}^{n}k_j\prod_{\substack{r=2 \\ r\neq j}}^{n}(k_{-r} - \lambda) = 0 \quad \text{(B3)}$$

λ is the eigenvalue; in general, there will be n λ_k's ($\lambda_k = 1/\tau_k$, τ_k = kth relaxation time). Division by $[\prod_{j=2}^{n}(k_{-j} - \lambda)]/\lambda$ and rearrangement yields

$$[k_1(a_1)/\lambda]\{1 + \sum_{j=2}^{n}[k_j/(k_{-j} - \lambda)]\} + k_{-1}/\lambda - \{1 + \sum_{j=2}^{n}[k_j/(k_{-j} - \lambda)]\} = 0 \quad \text{(B4)}$$

Equation B3 and the rearranged eq B4 are convenient forms of the characteristic equation from which some useful general properties predicted by the model can be deduced.

Let $Q = 1 + \sum_{j=2}^{n}[k_j/(k_{-j} - \lambda)]$ and $R = k_{-1}/\lambda$.

(*a*) *Any Given Intercept Value of* λ (λ_{int}) *Occurs Once and Only Once.* Proof: As the concentrations of the initial reactants decrease to zero ($a_1 = 0$), then $R - Q = 0$. Because the relaxation times and the reverse rate constants are real and positive, R must be positive. Assume that $\lambda(a_1) = \lambda(0)$ for values of a_1 intermediate between 0 and ∞. Since λ_{int} satisfies the equation $R - Q = 0$ and $k_1(a_1) \neq 0$, then $\lambda(a_1)$ can only be equal to the intercept value if $Q = 0$; but this is a contradiction of $R - Q = 0$.

(*b*) *There Exists Only One Eigenvalue Which Increases without Limit at Large Concentrations of Reactants; All Other Eigenvalue Functions* λ_i *Possess a Plateau Value Whose Limit Cannot Exceed the Intercept Value of* λ_{i-1}. Proof: Inspection of the characteristic equation reveals that, as $a_1 \rightarrow \infty$, λ (which is defined for convenience as λ_1) reduces to $k_1(a_1)$, which increases with a_1, i.e., without bound. The intercept of λ_1 defines an upper limit for the next largest eigenvalue λ_2 by (a) above, and by extension, the intercept of each λ_{i-1} defines the upper limit for the plateau value of λ_i.

(*c*) *Reciprocal Relaxation Times Are Monotonically Increasing Functions of Free Concentrations of Reactants.* Proof: For the unbounded eigenvalue this is obvious. Hence, it remains to show that (c) is true for all remaining bounded λ_i's. Taking the derivative of λ times eq B4 yields

$$\lambda'\{Q - [k_1(a_1 - \lambda)]\sum_{j=2}^{n}k_j/(k_{-j} - \lambda)^2\} = k_1Q \quad \text{(B5)}$$

with $\lambda' = d\lambda/d(a_1)$. As before, at large reactant concentrations $Q = 0$; eq B5 reduces to

$$\lambda'[k_1(a_1)\sum_{j=2}^{n}k_j/(k_{-j} - \lambda)^2] = 0 \quad \text{(B6)}$$

and is true for $\lambda' = 0$. At the intercept, $a_1 = 0$ and $Q = R$.

Therefore, λ' is equal to a nonzero positive number; see eq B5. We ask if $\lambda' = 0$ for the bounded eigenvalues at any other value between the intercept ($a_1 = 0$) and the plateau region ($a_1 \rightarrow \infty$). According to eq B5, λ' can be zero only if $Q = 0$ or if $\lambda = k_{-j}$. At intermediate values of a_1, Q cannot = 0 as the characteristic eq B4 would lead to the contradiction that $R = 0$. Analogously, the characteristic equation does not hold if $Q = \infty$, which occurs when $\lambda = k_{-j}$. Therefore, the bounded λ's begin with a positive slope at the intercept and monotonically increase to the plateau values where $\lambda' = 0$ at high reactant concentrations.

Summary of Appendix B. As for the parallel and series kinetic schemes analyzed by Clegg (1984), the branched series model, in general, consists of an ordered set of eigenvalues such that $\lambda_1 > \lambda_2 > \ldots \lambda_n$. λ_1 is unbounded and increases linearly with the reactant concentrations. All other λ_i ($i \neq 1$) are increasing monotonic functions of the reactant concentrations rising from some intercept value to a plateau value that is bounded by the intercept value of λ_{i-1}.

(C) The linear differential equations describing the rate of change of the excited-state species concentrations in Scheme II can be written as

$$d[Pro]^*/dt = -(k_e^{*s}[P_0] + k_{d1}^*)[Pro^*] + k_{-e}^{*s}[C_e^*]$$

$$d[C_e^*]/dt = k_e^{*s}[P_0][Pro^*] - (k_{-e}^{*s} + k_1^{*s} + k_{d2}^*)[C_e^*] + k_{-1}^{*s}[C_{int}^*] \quad (C1)$$

$$d[C_{int}^*]/dt = k_1^{*s}[C_e^*] - (k_{-1}^{*s} + k_{d3}^*)[C_{int}^*]$$

The approximation has been made that the concentration of DNA occupied by proflavin is negligible; i.e., $[P] = [P_0]$. It follows that $d[P_0]/dt = 0$. k_e^{*s} and k_{-e}^{*s} are the forward rate constants for the bimolecular step in the excited state; otherwise, the notation is the same as that found in the text concerning this scheme. The equations can also be expressed in matrix form:

$$-d/dt\,(\Delta\epsilon_3) = \begin{bmatrix} (k_e^{*s}[P_0] + k_{d1}^*) & -k_{-e}^{*s} & 0 \\ -k_e^{*s}[P_0] & (k_{-e}^{*s} + k_1^{*s} + k_{d2}^*) & -k_{-1}^{*s} \\ -k_1^{*s} & 0 & (k_{-1}^{*s} + k_{d3}^*) \end{bmatrix} \Delta\epsilon_3 \quad (C2)$$

where $\Delta\epsilon_3$ represents the column vector ($[Pro^*]$, $[C_e^*]$, $[C_{int}^*]$). The characteristic equation resulting from expansion of the eigenvalue determinant is a cubic equation in λ ($=1/\tau$). The three roots, λ_i ($i = 1, 2, 3$) as functions of the kinetic parameters and $[P_0]$, can be numerically evaluated.

If the first bimolecular kinetic step, characterized by K_e^* in Scheme II, is much faster then the subsequent monomolecular process, it is kinetically uncoupled to it, and the linear differential equations become

$$d[Pro^*]/dt = -\{(k_{d1}^* + (k_1^{*s} + k_{d2}^*)K_e^{*s}[P_0])[Pro^*] - k_{-1}^{*s}[C_{int}^*]\}/\{1 + K_e^{*s}[P_0]\}$$

$$d[C_{int}^*]/dt = k_1^{*s}K_e^{*s}[P_0][Pro^*] - (k_{-1}^{*s} + k_{d3}^*)[C_{int}^*] \quad (C3)$$

or in matrix form

$$-d/dt\,(\Delta\epsilon_2) = \begin{bmatrix} \{k_{d1}^* + (k_1^{*s} + k_{d2}^*)K_e^{*s}[P_0]\}/\{1 + K_e^{*s}[P_0]\} & -k_{-1}^{*s}/\{1 + K_e^{*s}[P_0]\} \\ -k_1^{*s}K_e^{*s}[P_0] & k_{-1}^{*s} + k_{d3}^* \end{bmatrix} \Delta\epsilon_2 \quad (C4)$$

where $\Delta\epsilon_2$ represents the column vector ($[Pro^*]$, $[C_{int}^*]$). The corresponding characteristic equation resulting from expansion of the eigenvalue determinant is a quadratic in λ, the solution of which yields two eigenvalues, λ_1 and λ_2, which are functions of the kinetic parameters and $[P_0]$.

Registry No. Poly[d(A-T)], 26966-61-0; poly[d(A-br^{5}U)], 51853-70-4; proflavin hemisulfate, 553-30-0.

References

Albert, A. (1966) *The Acridines*, 2nd ed., p 193, Edward Arnold Ltd., London.

Albert, A. (1973) *Selective Toxicity*, 2nd ed., Chapman & Hall, London.

Austin, R. H., Chan, S. S., & Jovin, T. M. (1979) *Proc. Natl. Acad. Sci. U.S.A. 76*, 5650–5654.

Avery, L. (1982) *J. Chem. Phys. 76*, 3242–3248.

Brenner, S., Barnett, L., Crick, F. H. C., & Orgel, A. (1961) *J. Mol. Biol. 3*, 121–124.

Cairns, J. (1962) *Cold Spring Harb. Symp. Quant. Biol. 27*, 311–318.

Caspersson, T., Zech, L., Modest, E. J., Foley, G. E., Wagh, U., & Simonsson, E. (1969) *Exp. Cell Res. 58*, 141–152.

Castellan, G. W. (1963) *Ber. Bunsen-Ges. Phys. Chem. 67*, 898–908.

Clegg, R. M. (1984) *J. Chem. Phys. 81*, 5546–5551.

Corin, A. F., Matayoshi, E. D., & Jovin, T. M. (1985) in *Spectroscopy and the Dynamics of Biological Systems* (Bayley, P. M., & Dale, R. E., Eds.) pp 53–78, Academic, London.

Corin, A. F., Blatt, E., & Jovin, T. M. (1986) *Biochemistry* (in press).

Dourlent, M., & Hogrel, J. F. (1976) *Biochemistry 15*, 430–436.

Eigen, M., & DeMaeyer, L. (1974) in *Techniques of Chemistry* (Weissberger, A., Ed.) Vol 6, Part II, pp 63–146, Wiley-Interscience, New York.

Galley, W. C., & Purkey, R. M. (1972) *Proc. Natl. Acad. Sci. U.S.A. 69*, 2198–2202.

Geacintov, N. E., Waldmeyer, J., Kuzmin, V. A., & Kolubayev, T. (1981) *J. Phy. Chem. 85*, 3608–3613.

Gill, J. E., Mazrimas, J. A., & Bishop, C. C. (1974) *Biochim. Biophys. Acta 335*, 330–348.

Guillain, F., & Thusius, D. (1970) *J. Am. Chem. Soc. 92*, 5534–5536.

Inman, R. B., & Baldwin, R. L. (1962) *J. Mol. Biol. 5*, 172–184.

Johnson, P., & Garland, P. B. (1981) *FEBS Lett. 132*, 252–256.

Johnson, P., & Garland, P. B. (1982) *Biochem. J. 203*, 313–321.

Jovin, T. M. (1975) in *Biochemical Fluorescence Concepts* (Chen, R. F., & Edelhoch, H., Eds.) Vol. I, pp 305–374, Dekker, New York.

Jovin, T. M., Bartholdi, M., Vaz, W. L. C., & Austin, R. H. (1981) *Ann. N.Y. Acad. Sci. 366*, 176–196.

Kapuscinski, J., & Darzynkiewicz, Z. (1984) *J. Biomol. Struct. Dyn. 1*, 1485–1499.

Kapuscinski, J., Darzynkiewicz, Z., & Melamed, M. R. (1982) *Cytometry 2*, 201–211.

Lerman, L. S. (1961) *J. Mol. Biol. 3*, 18–30.

Lerman, L. S. (1963) *Proc. Natl. Acad. Sci. U.S.A. 49*, 94–102.

Li, H. J., & Crothers, D. M. (1969) *J. Mol. Biol. 39*, 461–477.

Luzzati, V., Mason, F., & Lerman, L. S. (1961) *J. Mol. Biol. 3*, 634–639.

Macgregor, R. B., Clegg, R. M., & Jovin, T. M. (1985) *Biochemistry 24*, 5503–5510.

Marcandalli, B., Winzek, C., & Holzwarth, J. F. (1984) *Ber. Bunsen-Ges. Phys. Chem. 88*, 368–374.

Marcandalli, B., Knoche, W., & Holzwarth, J. F. (1986) *Gazz. Chim. Ital.* (in press).

Matayoshi, E. D., Corin, A. F., Zidovetski, R., Sawyer, W. H., & Jovin, T. M. (1983) in *Mobility and Recognition in Cell Biology* (Sund, H., & Veeger, C., Eds.) pp 119–134, de Gruyter, Berlin and New York.
Mauss, Y., Chambron, J., Daune, M., & Benoit, H. (1967) *J. Mol. Biol. 27*, 579–589.
Neidle, S., & Berman, H. M. (1983) *Prog. Biophys. Mol. Biol. 41*, 43–66.
Nelder, J. A., & Mead, R. (1964) *Comput. J. 7*, 308–313.
Pachmann, U., & Rigler, R. (1972) *Exp. Cell Res. 72*, 602–608.
Parker, C. A. (1968) *Photoluminescence of Solutions*, pp 1–544, Elsevier, Amsterdam.
Parker, C. A., & Joyce, T. A. (1973) *Photochem. Photobiol. 18*, 467–474.
Parker, C. A., Hatchard, C. G., & Joyce, T. A. (1964) *J. Mol. Spectrosc. 14*, 311–319.
Peacocke, A. R. (1973) in *Acridines* (Acheson, R. M., Ed.) p 723, Interscience, New York.
Porumb, H. (1978) *Prog. Biophys. Mol. Biol. 34*, 175–195.
Post, C. B., & Zimm, B. H. (1982) *Biopolymers 21*, 2139–2160.
Provencher, S. V. (1976a) *Biophys. J. 16*, 27–41.
Provencher, S. V. (1976b) *J. Chem. Phys. 64*, 2772–2777.
Ramstein, J., & Leng, M. (1975) *Biophys. Chem. 3*, 234–240.
Ramstein, J., Dourlent, M., & Leng, M. (1972) *Biochem. Biophys. Res. Commun. 47*, 874–882.
Ramstein, J., Houssier, C., & Leng, M. (1973) *Biochim. Biophys. Acta 335*, 54–68.
Ramstein, J., Ehrenberg, M., & Rigler, R. (1980) *Biochemistry 19*, 3938–3948.
Rigler, R., & Ehrenberg, M. (1973) *Q. Rev. Biophys. 6*, 139–199.
Rigler, R., Rabl, C.-R., & Jovin, T. M. (1974) *Rev. Sci. Instrum. 45*, 580–588.
Ryan, D. P., & Crothers, D. M. (1984) *Biopolymers 23*, 537–562.
Streisinger, G., Okada, Y., Emrich, J., Newton, J., Tsugita, A., Terzaghi, E., & Inouye, M. (1966) *Cold Spring Harbor Symp. Quant. Biol. 31*, 77–84.
Thusius, D. (1977) *Biophys. Chem. 7*, 87–93.
van de Sande, H., & Jovin, T. M. (1982) *EMBO J. 1*, 115–120.
Widom, J., & Baldwin, R. L. (1983) *Biopolymers 22*, 1595–1620.

Factor VII Binding to Tissue Factor in Reconstituted Phospholipid Vesicles: Induction of Cooperativity by Phosphatidylserine†

Ronald Bach,‡ Rodney Gentry,§ and Yale Nemerson*,‡

Division of Thrombosis Research, Department of Medicine, Mt. Sinai School of Medicine of The City University of New York, New York, New York 10029, and Department of Mathematics and Statistics, University of Guelph, Guelph, Ontario, Canada N1G 2W1

Received May 30, 1985; Revised Manuscript Received January 24, 1986

ABSTRACT: The binding of factor VII and tissue factor produces a membrane-associated proteolytic complex which may be the primary biological initiator of coagulation. Homogeneous tissue factor, a glycoprotein purified from bovine brain, was reconstituted into phospholipid vesicles ranging from neutral (100% phosphatidylcholine) to highly charged (40% phosphatidylserine) with octyl glucoside. The vesicles were characterized with respect to size and tissue factor content and orientation. Employing data from protease digestion, we deduced that tissue factor is randomly oriented; thus, its effective concentration in these vesicles was half its total concentration. In all binding experiments, 1 mol of enzyme was bound per mole of available activator at saturation. This stoichiometry was not affected by the form of the enzyme employed or the phospholipid composition of the vesicles. With tissue factor incorporated into phosphatidylcholine vesicles, the K_d was 13.2 ± 0.72 nM for factor VII and 4.54 ± 1.37 nM for factor VIIa. Thus, the one-chain zymogen binds to the activator with only slightly less affinity than the more active two-chain enzyme. Active-site modification of factor VII and factor VIIa with diisopropyl fluorophosphate resulted in tighter binding of the derivatized molecules. Inclusion of phosphatidylserine in the vesicles altered the binding both quantitatively and qualitatively. With increasing acidic phospholipid, the concentration of enzyme required to occupy half the activator sites was decreased. In addition, positive cooperativity was observed, the degree of which depended on the vesicle charge and the form of the enzyme. An explicit two-site cooperative binding model is presented which fits these complex data. In this model, tissue factor is at least a dimer with two interacting enzyme binding sites.

The initiation of coagulation by tissue factor was first demonstrated more than a century ago when it was shown that contact between damaged tissue and blood promoted rapid clot formation (de Blainville, 1834). Biochemical characterization of this thromboplastic activity began with the experiments of Howell (1912), who separated tissue thromboplastin into lipid and protein components, which by themselves were essentially inactive. Chargaff (1948) further characterized the lipid and protein fractions and showed that recombination under the appropriate conditions reconstituted the procoagulant activity. Thus, tissue factor was correctly identified as a lipoprotein. We have previously purified tissue factor to homogeneity from bovine brain (Bach et al., 1981). The molecule is a 41-kilo-

† Supported, in part, by Grant HL 29019 from the National Institutes of Health and Grant A9100 from NSERC, Canada.
‡ Mt. Sinai School of Medicine of The City University of New York.
§ University of Guelph.

0006-2960/86/0425-4007$01.50/0